J. Fluid Mech. (2005), *vol.* 530, *pp.* 327–352.
doi:10.1017/S0022112005003824 Printed in the United Kingdom

An experimental and numerical study of channel flow with rough walls

By P.-Å. KROGSTAD, H. I. ANDERSSON, O. M. BAKKEN AND A. ASHRAFIAN

Department of Energy and Process Engineering, Norwegian University of Science and Technology, N-7491 Trondheim, Norway

(Received 21 April 2004 and in revised form 9 December 2004)

A fully turbulent channel flow with smooth and rod-roughened walls has been investigated using hot-wire anemometry and direct numerical simulations (DNS). The mean flow follows the law of the wall for both surfaces and the velocity defect suggests that the outer layer is very little affected by the roughness. The Reynolds stresses appear to be very similar for the two surface geometries outside $y \approx 5k$, where k is the roughness height. A quadrant analysis shows that the structural differences close to the wall extend somewhat further out. The turbulence structure is further investigated using stress ratios and the anisotropy tensor, which corroborate the findings from the Reynolds stresses. Many of the recent investigations on boundary layers seem to find large differences between smooth and rough wall data in the outer layer also. A tentative explanation for the apparent dependence on flow type of the surface roughness effects is given.

1. Introduction

Turbulent flows over smooth surfaces have been studied extensively for a long time, both experimentally and theoretically. The importance of the wall layer was convincingly demonstrated experimentally by Kline *et al.* (1967). With the introduction of direct numerical simulations (DNS) considerably more detailed information has become available. Using this research tool, the mechanisms involved in the generation of self-sustained turbulent motion near the wall are now quite well understood (see e.g. Jimenez & Moin 1991) and the communication between the inner and outer layers has been elucidated.

Despite its significant importance in industrial applications, much less knowledge exists for flows over rough surfaces. In the limit of infinite Reynolds numbers all real surfaces will behave as rough walls and the details of the wall may significantly affect the characteristics of the flow. The effect of the modified surface topography on the mean velocity profile is well documented (see e.g. Townsend 1976, or the review article by Raupach, Antonia & Rajagopalan 1991). It is commonly assumed that the wall roughness is a local effect that only affects the inner layer up to a distance of about 4 to 5 roughness heights. In this roughness sublayer the roughness elements will interact strongly with the streamwise vortices found near the walls, so the inner region is expected to be severely modified compared to a smooth wall flow. In the outer layer, however, the flow is expected to be unaffected by the mechanism that produces the turbulence in the inner layer and therefore should behave similarly in rough and smooth wall flows.

The assumption that the wall effect is limited to a certain number of roughness element heights leads to the argument that in the fully rough case the inner layer should be modified from the smooth wall relation

$$U^+ = \frac{1}{\kappa} \ln y^+ + A \tag{1.1}$$

to the form

$$U^+ = \frac{1}{\kappa} \ln \left(\frac{y}{k} \right) + B(k^+), \quad B(k^+) = A - \Delta U^+ + \frac{1}{\kappa} \ln k^+, \tag{1.2}$$

where U is the mean velocity in the streamwise direction, y is the distance from the surface and κ is the von Kármán constant. A is the smooth wall constant and ΔU^+ is the modification of this constant due to roughness effects and is frequently called the 'roughness function'. (The $^+$ superscript indicates normalization with the friction velocity $u_\tau = \sqrt{\tau_w/\rho}$ or the viscous length scale ν/u_τ, where τ_w, ν and ρ are the wall shear stress, kinematic viscosity and density, respectively.) k is a measure of the roughness length scale, frequently taken as a convenient geometric length relevant to the roughness elements. A popular alternative is 'the equivalent sand roughness' which is the length scale which would produce the same ΔU^+ if the surface were covered by sieved sand. This has been found to produce the shift

$$\Delta U^+ = \frac{1}{\kappa} \ln k_s^+ + A - C, \tag{1.3}$$

where $C \approx 8.5$ (see e.g. Krogstad, Antonia & Browne 1992).

Only in very rare cases will the surface geometry be defined well by using only one length scale. Thus it is evident that k is generally not a well-defined flow quantity and its numerical value is only relevant when comparing flows over geometrically identical surfaces. However, once ΔU^+ is known, k may be related to the equivalent sand roughness which is given by

$$\frac{k_s}{k} = \frac{\exp[\kappa(\Delta U^+ - A + C)]}{k^+}. \tag{1.4}$$

An obvious difference between (1.1) and (1.2) is that the length scales used to normalize y in the two cases are fundamentally different. In (1.1) the scale used will depend on the Reynolds number and streamwise position, while the length scale in (1.2) is a constant.

The assumption about an outer layer which is unaffected by the wall condition implies that the velocity defect function

$$U_e^+ - U^+ = \frac{1}{\kappa} \ln \left(\frac{y}{\delta} \right) + \frac{2\Pi}{\kappa} [1 - w(y/\delta)] \tag{1.5}$$

must be the same for rough and smooth walls where $w(y/\delta)$ is the velocity wake function, here defined to be 1 at the outer edge of the layer, where $y = \delta$ and $U = U_e$, and Π is the wake strength which may vary with x. This assumption was questioned by Krogstad *et al.* (1992) in the case of boundary layers, based on the observation that Π derived from the rough wall layer was considerably higher than that in the smooth case.

In a zero-pressure-gradient boundary layer the momentum integral equation reduces to

$$\frac{\partial \theta}{\partial x} = \frac{C_f}{2}, \tag{1.6}$$

where θ is the momentum thickness. With a skin friction coefficient, C_f, which in the rough case may be 3 to 4 times as high as for a smooth wall layer, it is evident that the layer growth rate is much higher in the rough case. That implies a higher entrainment rate, which leads to an increase in Π as suggested by Krogstad *et al.* (1992). They therefore conjectured that the communication between the inner and outer layers over a rough wall must be much stronger than implied by the 'wall similarity' hypothesis of Townsend (1976).

However, the experimental evidence that the outer flow is directly modified by the surface roughness is not conclusive. Tani (1987) analysed a number of rough wall experiments and found the wake strength to be higher than for a smooth wall. The same was found by Poggi, Porporato & Ridolfi (2003). Tachie, Bergstrom & Balachandar (2000), who measured the turbulent boundary layer developing over rough walls generated by sand grains or a perforated plate, found that Π "varies significantly with the type of surface roughness". On the other hand, Song & Eaton (2002) found the wake strength to be virtually unaffected by the surface condition. (This has also been stated by other investigators, but in many of these cases a smooth wall value of Π has been used implicitly in the method of deriving C_f.) So far no DNS results have been published for rough wall boundary layers, but large-eddy simulation (LES) data have started to appear (e.g. Lee 2002; Tamura *et al.* 2003).

The Achilles heel of boundary layer experiments on rough surfaces has been the accurate determination of u_τ (see e.g. Krogstad *et al.* 1992). In most cases u_τ has been determined by a profile matching technique, which has proven very accurate for smooth surfaces. However, in the rough wall case the uncertainty is much higher, since both the exact location of the surface and the roughness function ΔU^+ are also unknown. Therefore the uncertainty about the effects of surface roughness may partly be due to inaccurate determination of u_τ.

In channel flows, on the other hand, u_τ may be obtained quite accurately since it is directly linked to the streamwise pressure gradient which is relatively easy to measure. Studies of roughness effects in channel flows may therefore help reduce the uncertainty in the results and thus enable firmer conclusions to be drawn. However, in the channel flow the conditions are somewhat different than for the boundary layer. There is no entrainment into the outer layer and the flow is always driven by a favourable pressure gradient. Both these circumstances lead to a reduced wake strength in the outer layer. Therefore there is little possibility for the velocity defect profiles to be different in the rough and smooth wall cases. Coupled to the fact that the shear stress distribution over most of the channel is directly linked to the pressure drop, the turbulent production (properly normalized) cannot be very different in the outer layers of smooth and rough wall channel flows. Also, the outer layer length scale (i.e. the channel half-height, h) is constant and the friction coefficient is independent of position in both the smooth and rough wall cases (assuming fully developed flow), so both the length scale ratios h/k and $h^+ = hu_\tau/\nu$ are independent of streamwise position. Therefore a streamwise equilibrium exists in both cases in the channel flow. This is not the case for boundary layers, where the thickness, δ, grows downstream. In the rough case C_f is virtually constant while over a smooth wall it decreases downstream. The scale ratio δ^+ will therefore develop differently along the two walls and an equilibrium type of flow will in general not exist in a boundary layer (although Smalley, Antonia & Djenidi 2001 have shown that the rough wall boundary layer ought to be a better candidate for similarity than the smooth wall case).

These two distinguishing features between boundary layers and channel flows (i.e. lower importance of the wake in the channel flow and difference in streamwise

development of inner scales) suggest that internal and external flows over rough walls may behave differently.

Fully developed flow in rough wall channels has recently been investigated by means of DNS. An attractive feature of this flow configuration from a computational point of view is that periodic boundary conditions can be used in the streamwise and spanwise directions. In the pioneering study of Miyake, Tsujimoto & Agata (2000), sand-grain roughness was represented by simplified roughness elements on one of the channel walls. Shortly thereafter, DNS of turbulent channel flow with transverse bar roughness were performed by Miyake, Tsujimoto & Masaru (2001), Ikeda & Durbin (2002), Leonardi *et al.* (2003, 2004) and Nagano, Hatori & Houra (2004). Leonardi *et al.* (2003) considered square-bar roughness with a wide range of pitch-to-height ratios, whereas Nagano *et al.* (2004) also studied rectangular rods 2 and 4 times wider than their height k. Ikeda & Durbin (2002) performed DNS of a configuration with uneven rod height.

A common feature of all these simulations was that only one of the channel walls was roughened while the other wall remained smooth. In some of these studies the one-sided roughness was partly motivated by the laboratory experiments of Hanjalic & Launder (1972), in which intentionally only one channel wall was roughened in order to produce an asymmetric mean flow field. Another characteristic of these DNS studies is that the roughness elements are relatively high, typically between 10% and 20% of the channel half-height, h, i.e. the blockage effect is substantial. According to Jimenez (2004), however, the channel half-height should be at least $40\,k$ in order to eliminate the direct effect of the roughness elements on the outer flow. This suggests that k should not exceed 2.5% of h.

The present paper reports on a combined experimental and computational investigation in which laboratory measurements and DNS data obtained from the same rough channel configuration are examined. In this study both walls are roughened by means of equally spaced square rods. The symmetry of the channel configuration makes the mean velocity field and the turbulence statistics symmetric and these symmetry properties may serve as a valuable check on the experimental and numerical data. Also, there is no ambiguity about the friction velocity to be used for scaling, since it is the same on both walls. Another distinguishing feature of the flow configuration to be considered is that the blockage effect is relatively small since the height of the roughness elements is only 3.4% of the channel half-height, i.e. smaller by a factor of 3 than in the earlier DNS of rod-roughened channel flow.

The outline of the paper is as follows. The flow configuration is described in the next section, together with some basic definitions and equations. Experimental and numerical aspects are presented in §§ 3 and 4, respectively. Section 5 presents a comparison of the mean velocity profiles and turbulent stresses obtained in smooth and rough wall channels. In § 6 the effect on the turbulence structure is investigated in more detail using quadrant analysis and anisotropy invariants. The main conclusions of this comparative study are provided in § 7.

2. Channel flow configuration

Laboratory experiments and computer simulations were conducted for pressure-driven flow in a plane channel. The top and the bottom walls were both equipped with transverse square rods of height k in a non-staggered arrangement. The centreline distance between two neighbouring rods was p, as indicated in figure 1. This flow configuration therefore exhibits three different geometrical length scales: h, k and p. In

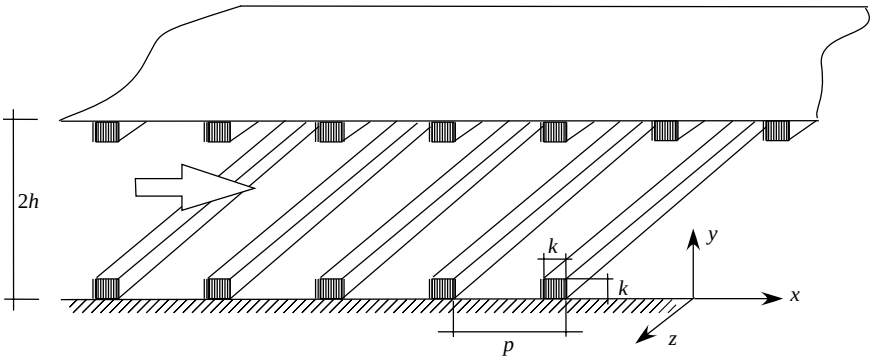

FIGURE 1. Channel definitions.

the present study the particular case $h/k = 29.4$ and $p/k = 8.0$ is considered. With the computer resources available this h/k ratio was the closest to the recommendations of Jimenez (2004) that could be obtained. A pitch-to-height ratio of $p/k = 8$ was chosen because it is known to cause the largest effect (i.e. shift ΔU^+) on the mean velocity profile (1.2) according to the boundary layer experiments of Furuya, Miyata & Fujita (1976) and the more recent channel simulations by Leonardi *et al.* (2003).

The turbulent flow of a Newtonian fluid with constant properties (ρ and μ) is governed by the incompressible Navier–Stokes equations and mass conservation. Whereas the instantaneous velocity vector $\tilde{\boldsymbol{u}} = (\tilde{u}, \tilde{v}, \tilde{w})$ and pressure $\tilde{p}$ are intrinsically time-dependent and three-dimensional, the corresponding Reynolds-averaged fields $\boldsymbol{U} = (U, V, 0)$ and P are steady and two-dimensional since the flow is statistically homogeneous both in time and in the spanwise z-direction.

The flow is driven solely by an imposed (negative) mean pressure gradient $\Delta P/\Delta x$ in the streamwise direction (see figure 1) from which the characteristic velocity scale u_τ is defined:

$$u_\tau^2 = -\frac{h}{\rho}\frac{\Delta P}{\Delta x}. \tag{2.1}$$

It should be emphasized that $\Delta P/\Delta x$ is required to overcome both the viscous shear and the form drag, i.e. the entire flow resistance. Moreover, unlike in turbulent boundary layers (cf. § 1), u_τ as defined in (2.1) does not vary with x except for the rod-induced periodic variations.

The equation governing mean streamwise momentum ρU can now be expressed in dimensionless form as

$$\begin{aligned}\frac{\partial}{\partial x^+}\left(U^{+2}\right) + \frac{\partial}{\partial y^+}(U^+V^+) \\ = -\frac{\partial P^+}{\partial x^+} + \frac{\partial}{\partial x^+}\left(2\frac{\partial U^+}{\partial x^+} - \overline{u^{+2}}\right) + \frac{\partial}{\partial y^+}\left(\left(\frac{\partial U^+}{\partial y^+} + \frac{\partial V^+}{\partial x^+}\right) - \overline{u^+v^+}\right),\end{aligned} \tag{2.2}$$

where the overbar denotes time averaging.

In the absence of roughness elements, i.e. in a smooth channel, $V^+ = 0$ and the dependent variables become independent of x. Thus, (2.2) simplifies to

$$0 = Re_\tau^{-1} + \frac{\mathrm{d}}{\mathrm{d}y^+}\left(\frac{\mathrm{d}U^+}{\mathrm{d}y^+} - \overline{u^+v^+}\right), \tag{2.3}$$

where $Re_\tau = u_\tau h/\nu$. In the rough wall case considered herein, the flow is fully developed in the streamwise direction in the sense that the dependent variables in (2.2) exhibit a quasi-periodic variation in the x-direction with periodicity p. By averaging (2.2) in x we obtain

$$0 = Re_\tau^{-1} + \frac{\mathrm{d}}{\mathrm{d}y^+}\left(\frac{\mathrm{d}\langle U^+\rangle}{\mathrm{d}y^+} - \langle\overline{u^+v^+}\rangle - \langle U^+V^+\rangle\right), \tag{2.4}$$

where the angle brackets $\langle\ \rangle$ denote streamwise averaging. Here, $-\langle U^+V^+\rangle$ represents the vertical transport of mean streamwise momentum ρU caused by the roughness elements. If (2.4) is integrated from an arbitrary position y^+ to the channel centre h^+ (notice that $h^+ = Re_\tau$), we obtain a linear variation

$$\frac{\mathrm{d}\langle U^+\rangle}{\mathrm{d}y^+} - \langle\overline{u^+v^+}\rangle - \langle U^+V^+\rangle = 1 - \frac{y^+}{h^+}. \tag{2.5}$$

The contributions to the apparent shear on the left-hand side of (2.5) are the viscous and the turbulent shear stresses, and the momentum loss influence caused by the periodic mean flow variation. Thus, outside the region where the impact of the roughness elements on the mean flow field is felt, the sum of the viscous and turbulent stresses varies linearly with y^+, as in a smooth channel.

The fully developed flow in a rod-roughened channel is a three-parameter problem. Here, the length scale ratios h/k and p/k are identical in the experiments and the computations. Ideally, the third parameter Re_τ should also have been the same. However, to ensure sufficient accuracy, the Reynolds number could not be lower than about 600 in the laboratory study (see § 3) while Re_τ could not exceed 400 in the DNS (see § 4). Moser, Kim & Mansour (1999) showed that some low-Re effects still remain in this Reynolds number range and such effects have been further addressed by Abe, Kawamura & Matsuo (2001). To facilitate sound interpretations of the rough wall data with respect to possible Re_τ effects between the experiment and the DNS, the smooth channel data of Moser *et al.* (1999) for $Re_\tau = 590$ are also provided.

3. Experimental details

Measurements were performed in a closed return wind tunnel with a working section consisting of two parallel plates forming a rectangular channel. The test section was 5 m long, with an inlet area of $1.35\,\mathrm{m} \times 0.10\,\mathrm{m}$. Measurements of velocity profiles at several spanwise locations were performed to verify that the aspect ratio was sufficiently large for the mean flow to be two-dimensional.

The flows along the ceiling and floor were tripped at the inlet using a 3 mm diameter rod followed by a 12 cm strip of No. 40 grit sandpaper, both spanning the width of the section. In the case of the rough surface, the ceiling and floor were covered with square bars $k \times k = 1.7 \times 1.7\,\mathrm{mm}^2$ spanning the whole width of the section.

A low-velocity calibration jet was used for the calibration of the hot wires. The reference velocity is determined from the pressure difference across an internal nozzle creating a large pressure drop even for low velocities. The nozzle is followed by several screens and a long diffusor of area ratio 11:1. The probe is placed and calibrated at the exit. The round jet produces a top-hat velocity profile with low turbulence intensity. The calibration rig was positioned on top of the channel and adjusted so that the jet flow was coaxial with the channel flow. A high-precision computer controlled traversing system was used for calibration and measurements. This system also enabled movement of the probes between the calibration rig and the channel

flow, so that the probes were never removed from the probe support or disconnected from the anemometer when shifting it between the calibration rig and the test section.

The hot wires were in-house-made single- and X-wire probes (using different probe designs for UV- and UW-measurements). The wires were partly etched 2.5 μm Wollaston Pt–10%Rh wire with an active length, l_w, of about 0.5 mm. The length to diameter ratio was thus close to 200 and the included angle of the two wires was nominally 100°. The separation between the wires was approximately the same as the active wire length.

The X-wires were calibrated using a velocity-dependent effective angle method. The method has the same benefits as a full velocity *vs.* yaw-angle calibration routine, but requires considerably less effort. The response of the wire is assumed to be of the form

$$U_{\text{eff}} = S\cos(\alpha + \gamma_{\text{eff}}), \tag{3.1}$$

where S is the norm of the velocity vector, α is the local flow angle and γ_{eff} is the effective wire inclination to the probe axis. This angle is normally taken to be a constant given by the probe geometry only. However, this has been shown not to be the case for very low velocities (see Bakken & Krogstad 2004). The probe is first calibrated for velocity with the probe aligned with the flow and a fourth-order polynomial is fitted to the velocity *vs.* voltage data. The probe is then calibrated for yaw sensitivity at a number of reference velocities covering the entire measurement range and a curve fit of γ_{eff} *vs.* S is made. During data reduction the velocity-dependent effective angle is determined on a sample-by-sample basis and the system of equations must be solved iteratively. Full details of this method may be found in Bakken & Krogstad (2004).

The hot wires were operated with in-house-made constant-temperature anemometers at an overheat ratio of 1.5. The filter frequencies of the low-pass filter, ($f_{\text{cut, rod}} = 1.5$ kHz and $f_{\text{cut, smooth}} = 2.5$ kHz) were adjusted after spectral investigation to match the highest Kolmogorov frequencies in the flows. About 6×10^5 samples were acquired to a PC using a National Instruments 16-bit A/D converter at sampling frequencies twice the cut-off frequencies. The temperatures in the calibration facility and in the wind tunnel were constantly monitored using thermocouples. The effect of temperature drift was corrected for using the method of Bearman (1971).

The dissipation rate, ϵ, was estimated using single wires assuming local isotropy and Taylor's hypothesis. The Kolmogorov length scale, $\eta = (\nu^3/\epsilon)^{1/4}$, varied from about 0.20 mm close to the wall to about 0.42 mm at the centreline in the smooth case, giving $(l_w/\eta)_{\max} \approx 2.5$. In the rough case the variation was from about 0.24 mm to about 0.47 mm, so that $(l_w/\eta)_{\max} \approx 2.1$. Hence the data are assumed to be very little affected by probe resolution errors.

Determination of the friction velocity, u_τ, is usually straightforward in a channel flow using the mean pressure gradient (see (2.1)). In this study, the pressure drop was only of the order of 4 Pa for the whole length of the channel. Measurement uncertainties in this pressure range were too high to obtain reliable estimates of $\mathrm{d}P/\mathrm{d}x$. In the smooth case u_τ was estimated from the mean velocity profiles by matching the data to the DNS of Moser *et al.* (1999). A second independent estimate for u_τ was obtained from the linear part of the total shear stress profiles in (2.5) using the X-wire data. The two methods agreed to within about 1%. For the smooth wall single- and UW-wire measurements, estimates of u_τ could only be obtained from the mean velocity profiles. A very good collapse of the $\overline{u^{+2}}$ profiles from measurements

using the three different probes was observed in the smooth case for $y/h > 0.2$. The small difference found closer to the wall was due to differences in spatial resolution. Due to the unknown shift in the mean velocity profile in the rough case, the friction velocity could not be estimated from the mean velocity profile. Therefore, u_τ had to be deduced from the total shear stress profile, assuming the accuracy to be the same as in the smooth case. For the rough wall single- and UW-wire measurements u_τ was determined by matching the outer layer $\overline{u^{+2}}$ data to the profiles obtained with the UV-probe. Using these procedures the uncertainty in u_τ was estimated to be less than $\pm 4\%$.

4. Numerical procedure

A direct numerical simulation of turbulent flow in a plane channel was performed. The pitch-to-height ratio and the relative roughness height were exactly as in the accompanying laboratory study (see § 3). The fully developed flow was driven by a prescribed pressure gradient so that the Reynolds number Re_τ based on the friction velocity defined in (2.1) was 400.

4.1. *Numerical method*

The spatial and temporal evolutions of the turbulent flow field are completely described by mass continuity and the incompressible Navier–Stokes equations. The governing equations are solved using an explicit version of the fractional-step method proposed by Chorin (1968) on a staggered Cartesian non-uniform grid in which the pressure, $\tilde{p}$, is defined at the centre of each grid cell and the components of the velocity vector $\tilde{\boldsymbol{u}}$ at the interfaces of the grid cells. Velocity components and their derivatives, which have to be determined at locations between the corresponding locations of the former, are obtained by linear interpolation and central differences, respectively. As a result, the spatial discretization is of second-order accuracy.

Using a leapfrog scheme for the explicit time integration of the momentum equation (with a time-lagged diffusion term), a second-order accuracy in time is achieved by

$$\tilde{\boldsymbol{u}}^{n+1} = \tilde{\boldsymbol{u}}^{n-1} + 2\Delta t\left[N(\tilde{\boldsymbol{u}}^n) + \frac{1}{Re}\nabla^2\tilde{\boldsymbol{u}}^{n-1} - \nabla(\tilde{\boldsymbol{p}}^{n+1})\right], \tag{4.1}$$

where $N(\tilde{\boldsymbol{u}}^n)$ denotes the nonlinear terms. The pressure at the new time level $\tilde{p}^{n+1} = \tilde{p}^n + \Delta\tilde{p}^{n+1}$ is determined by the solution of the Poisson equation

$$\nabla^2(\Delta\tilde{p}^{n+1}) = \frac{1}{2\Delta t}\nabla\cdot\tilde{\boldsymbol{u}}^*, \tag{4.2}$$

where $\tilde{\boldsymbol{u}}^*$ is an intermediate velocity field, calculated by omitting the pressure term in (4.1). A divergence-free field $\tilde{\boldsymbol{u}}^{n+1}$ is obtained after a velocity correction

$$\tilde{\boldsymbol{u}}^{n+1} = \tilde{\boldsymbol{u}}^* - 2\Delta t\nabla(\Delta\tilde{p}^{n+1}). \tag{4.3}$$

The combination of central interpolation and a leapfrog time-step is energy conserving for the one-dimensional convection equation. This is the reason why it is especially suited for DNS. In combination with the diffusion operator, however, the leapfrog time-step is slightly unstable. Therefore, the diffusive term is taken at the time level $n-1$ in (4.1). Every 41 time steps, an averaging step is performed in order to prevent $2\Delta t$ oscillations inherent in the leapfrog time advancement. The Poisson equation (4.2) is solved by an iterative procedure accelerated by a multi-grid cycle. The smoother (single-grid iteration) is based on the velocity–pressure iteration presented by Hirt

et al. (1975) with over-relaxation. This scheme gives the same convergence properties as a conventional Gauss–Seidel iteration with successive over-relaxation (SOR). The advantage of the present algorithm is the easy treatment of boundaries, at which only velocity boundary conditions have to be specified. This has proven useful in simulating flow fields in arbitrary geometries with an immersed boundary method in Cartesian grids (Tremblay, Manhart & Friedrich 2001). The described procedure also has the advantage that during the iterations, full control over the residual divergence of the velocity field is obtained.

4.2. *Computational domain and resolution*

The length L_x and the width L_z of the computational domain were $6.528\,h$ and πh, respectively, i.e. essentially the same as in the smooth channel DNS at $Re_\tau = 395$ by Moser *et al.* (1999) and Abe *et al.* (2001). Alternatively, the length of the computational box can be expressed in terms of the roughness characteristics, i.e. $L_x = 24p = 192k$. Thus, the domain comprised 24 rods on each side of the channel. No-slip and impermeability conditions were imposed on the channel walls and on the faces of the square rods. The computational domain was believed to be sufficiently large so that periodic boundary conditions could be used both in the streamwise and spanwise directions.

A uniform distribution of grid points was used both in the streamwise and spanwise directions. In order to achieve an adequate resolution in the vicinity of the rods, Δx^+ was only 3.4 in wall units. In the innermost wall region, i.e. within $y < 3k$, a uniform grid spacing with $\Delta y^+ = 0.5\Delta x^+ = 1.7$ was used also in the wall-normal direction. Thus, the innermost node in which the streamwise velocity component was evaluated was located only 0.85 wall units away from the surface. Moreover, three nodes were located inside the viscous sublayer, as recommended by Grötzbach (1983) to ensure sufficient wall-normal resolution. Beyond $y = 3k$, Δy^+ was gradually increased towards the centre of the channel. The mean grid width $\Delta = (\Delta x \Delta y \Delta z)^{1/3}$ therefore increases monotonically from the near-wall region towards the mid-plane of the channel where $\Delta^+ \approx 7.5$. On the basis of the energy dissipation rate the Kolmogorov length scale can be estimated to be $\eta^+ = 2.5$. The criterion $\Delta < \pi\eta$ for sufficient grid resolution suggested by Grötzbach (1983) is therefore fulfilled. Similarly, the Kolmogorov time scale τ can be estimated to be about 6 viscous time units ν/u_τ^2, whereas the time step Δt used in the simulations corresponded to $\Delta t^+ = 0.16 \ll \tau^+$. This tiny time step was chosen to avoid numerical instabilities (Orellano & Wengle 2000) which may arise from the explicit time integration scheme employed.

4.3. *Initialization, data sampling and verification*

A three-dimensional initial flow field was obtained from a very-large-eddy simulation (VLES) of smooth channel flow with $Re_\tau = 400$. The mean velocity, however, was adjusted to the appropriate rough wall levels. This VLES was based on the most energetic POD modes deduced from an earlier large-eddy simulation. Small-scale modes were randomly imposed to ensure some energy in the high-wavenumber part of the spectrum (see Johansson & Andersson 2004 for details). In the presence of rods the DNS was first advanced forward in time until a realistic turbulent flow field evolved after a time corresponding to $2\,h/u_\tau$ and a statistically steady state was reached $3\,h/u_\tau$ later. The simulation continued for another $20\,h/u_\tau$, during which statistics were computed from individual flow fields equally separated $0.5\,h/u_\tau$ or 200 viscous units in time. In addition to averaging over these 40 nearly independent flow fields, averaging was also performed in the homogeneous spanwise direction. Since the roughness elements induced a streamwise periodicity of the averaged field, the statistical equivalence of two points (x, y, z) and $(x + np, y, z)$, where p is the pitch and n is

an integer, was utilized to further increase the number of statistically independent samples. To further increase the number of samples, averaging over both sides of the channel was also carried out, thus benefiting from the geometrical symmetry of the rod-roughened channel.

For comparative purposes a DNS of smooth channel flow also at $Re_\tau = 400$ was performed. The computations were carried out using $256 \times 192 \times 192$ grid points in a computational box of size $(L_x, L_y, L_z) = (6.528h, 2h, \pi h)$. The grid was uniform in the stream- and spanwise directions with resolutions $\Delta_x^+ \approx 9.8$ and $\Delta_z^+ = 6.5$, respectively. The first computational grid point was located at $y_1^+ = 0.7$ from the bottom wall. The computational characteristics were nearly the same as for the rough wall DNS, except that the grid spacing in the streamwise direction was larger than in the presence of the rods. The outcome of this simulation was compared with results of Abe *et al.* (2001) for $Re_\tau = 395$. The size of their computational box was practically the same as in the present case and their second-order finite-difference code was similar to the MGLET code used herein. The agreement between the present turbulence statistics and those of Abe *et al.* (2001) was generally very good (see Ashrafian & Andersson 2004).

5. Results

The smooth wall experiment was performed at $Re_\tau = 670$, corresponding to a bulk Reynolds number of $Re_b = U_b h/\nu = 12800$ (where U_b is the average velocity measured across the channel exit). Since we were unable to run our code at this Reynolds number, the DNS smooth wall reference used is the $Re_\tau = 590$, $Re_b = 10700$ simulation of Moser *et al.* (1999). For the flow in the rough wall channel the Reynolds numbers were $Re_\tau = 600$ and $Re_b = 6000$ for the experiment and $Re_\tau = 400$ and $Re_b = 4200$ in the DNS. Our own smooth wall DNS at $Re_\tau = 400$, $Re_b = 6300$ has also been included as reference for the rough wall DNS and to help estimate the Reynolds number effects expected between the rough wall DNS and experiment.

The relatively high value of h/k gave a roughness height, k^+ (i.e. in terms of the viscous length scale ν/u_τ) of $k^+ = 13.6$ for the DNS and $k^+ = 20.4$ in the experiment. From the estimated ΔU^+ (see below) the equivalent sand roughnesses could be calculated from (1.4). For the DNS k_s^+ was found to be $k_s^+ = 63$, while the experiment gave $k_s^+ = 121$. As a rule-of-thumb it is frequently assumed (see e.g. Raupach *et al.* 1991) that k_s^+ needs to be higher than about 70 for the flow to be considered fully rough, i.e. where the viscous shear at the wall may be neglected compared to the form drag produced by the roughness elements. Thus the DNS surface is transitionally rough while the experiment is conducted in the fully rough regime. However, just as the buffer layer matches asymptotically with the logarithmic region on a smooth surface at y^+ of about 70, the viscous effects disappear gradually as k_s^+ increases. This is clearly seen in the transitionally rough part of the Moody diagram. It is therefore believed that the effects of the transitional roughness in the DNS compared to a fully rough simulation must be quite small. This is further supported by the computed contributions to the surface drag from the pressure and viscous forces. The ratio was found to be close to 200 (Ashrafian, Andersson & Manhart 2004), implying that the DNS is also close to being in the fully rough regime.

5.1. *Mean velocity*

The mean velocity measured in the smooth wall channel ($Re_\tau = 670$) is plotted in inner variables in figure 2 together with the DNS data of Moser *et al.* (1999) at $Re_\tau = 590$

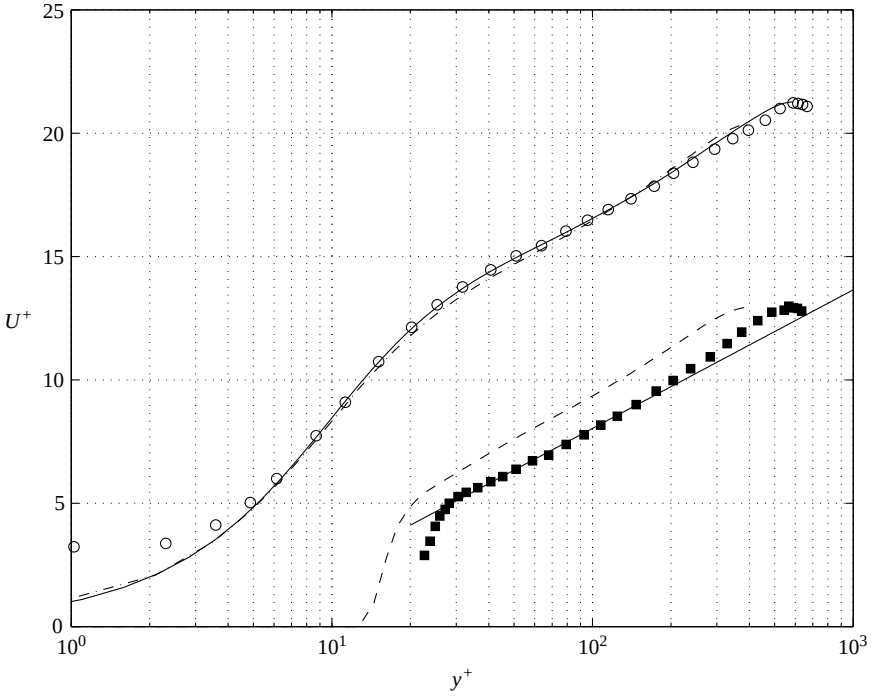

FIGURE 2. Mean velocity profiles. ———, Smooth channel DNS at $Re_\tau = 590$ (Moser *et al.* 1999); –·–·–, smooth channel DNS at $Re_\tau = 400$; ○, smooth channel experiment at $Re_\tau = 670$; – – –, rough wall DNS at $Re_\tau = 400$; ■, rough wall experiment at $Re_\tau = 600$. A solid line is used for comparison of the rough wall experiment with the log-law (1.1).

and the present smooth wall DNS data ($Re_\tau = 400$). The differences are seen to be very small. For $y^+ < 5$ the usual effect of the wall on the hot wire is seen as an increasing overestimate of U^+ as the wall is approached.

The mean velocity profiles above the crest of the roughness elements are also shown in figure 2. For the DNS the Re_τ is again 400, but for the experiment the lowest acceptable operating speed gave $Re_\tau = 600$. In all figures the distance is measured from the wall between the ribs (as indicated in figure 1). Figure 2 shows that in the case of rib-roughened surfaces, the flow exhibits a well-defined logarithmic layer using this reference position. This was also observed by Cui, Patel & Lin (2003) in their LES.

The wall roughness causes an increase in surface friction. The friction factor,

$$f = \frac{8\tau_w}{\rho U_b^2} = 8\left(\frac{u_\tau}{U_b}\right)^2,$$

was found to be $f = 0.073$ for the DNS and $f = 0.079$ in the experiment, respectively. This difference is well within the estimated uncertainty of u_τ. In a fully rough flow, f is expected to depend very little on the flow Reynolds number and the somewhat lower value of the DNS friction factor reflects a k^+ in the upper end of the transitional regime. The downward shift, ΔU^+, in the logarithmic part of the velocity distribution, (1.2), was found to be $\Delta U^+ = 7.1$ in the DNS, while the experiment gave $\Delta U^+ = 8.7$. The difference is due to the differences in Re_τ. If the flow is in the fully rough regime, the shift should follow the relation

$$\Delta U^+ = \frac{1}{\kappa}\ln k^+ + \text{const.} \tag{5.1}$$

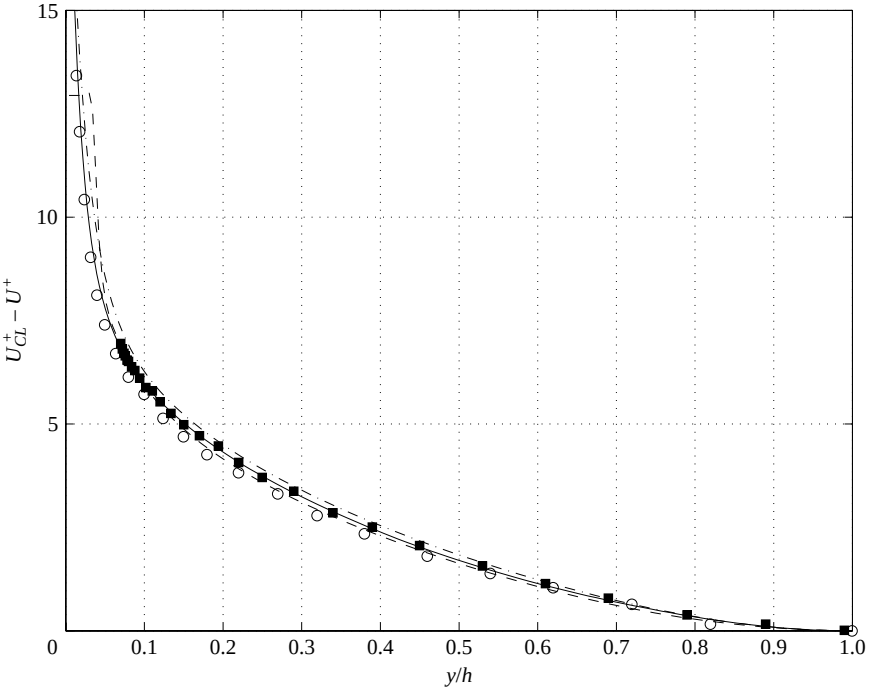

FIGURE 3. Velocity defect profiles. Symbols as in figure 2.

Assuming f to be independent of Re_τ, the experimental value of ΔU^+ at the Re_τ of the DNS would have been $\Delta U^+ = 7.4$. This very small difference is again reflected by the k_{DNS}^+ being in the upper part of the transitional regime. As conjectured in § 1, the velocity defect function was found to be virtually insensitive to the surface roughness (figure 3). Within the experimental scatter the smooth wall DNS and the measurements produce the same velocity defect. The rough wall DNS and measured velocity defects also agree well with the smooth wall data. Only very close to the crest of the roughness element may a small deviation from the smooth wall distribution be seen. This indicates that the effect of the roughness element on the velocity defect is limited to $y/h \leqslant 0.04$, which is only slightly above the crest of the roughness element.

Due to the errors introduced in the hot-wire measurements from the high turbulence level found near the cavity, no attempt was made to measure the mean velocity profile at places other than above the crest of the roughness element. The DNS shows that above $y/h > 0.17$ the mean velocity profiles are virtually independent of streamwise position (Ashrafian *et al.* 2004). However, below this limit the velocity is varying rapidly with distance from the wall and streamwise position, making the measurements close to the wall prone to positioning errors as well.

5.2. *Reynolds stresses*

Figure 4 shows that the measurement technique used was capable of reproducing the smooth wall streamwise normal stress, $\overline{u^{+2}}$, very well. The peak was found to be near $y^+ \approx 15$ in the experiment and is slightly underestimated, but for most of the cross-section the DNS and hot-wire data collapse. (The small shift in the location of the stress peak to lower y/h in the experiment is due to the difference in Re_τ.)

In the rough case the peak in $\overline{u^{+2}}$ is considerably reduced due to the break-up of the streamwise vortices. This has also been observed by other investigators (e.g. in

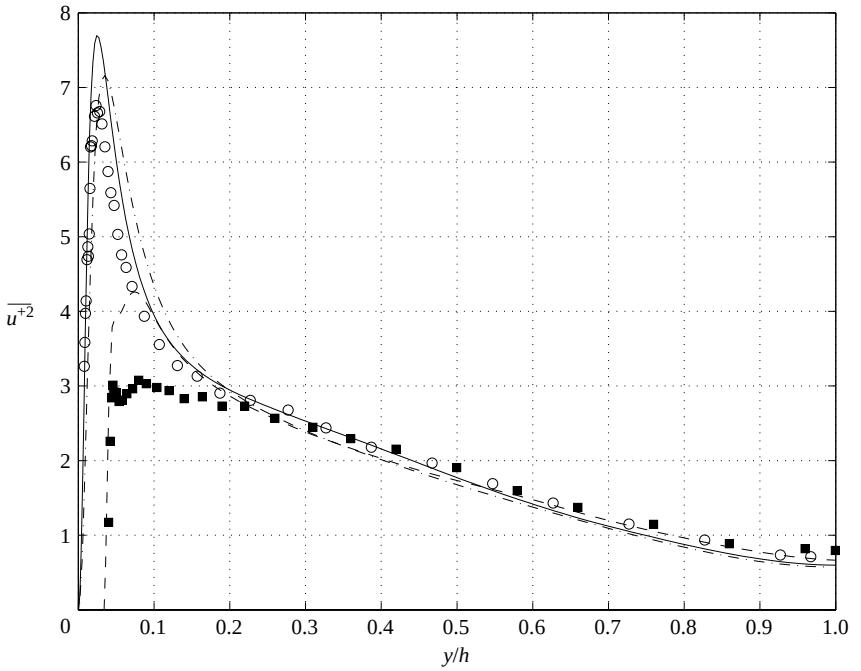

FIGURE 4. Streamwise normal stress profiles, $\overline{u^{+2}}$. Symbols as in figure 2.

the experiments of Grass 1971, Andreopoulos & Bradshaw 1981, Krogstad & Antonia 1999 and in the DNS of Miyake *et al.* 2000). The reduction observed in the experimental data appears to be overestimated compared to the DNS. This was shown by Bakken & Krogstad (2005) to be a Reynolds number effect, and they found that all traces of the near-wall peak were absent at $Re_\tau = 1200$. In the smooth case, the peak is mainly due to viscous effects. For the fully rough case, the pressure-induced drag completely dominates the drag, leaving no region of viscous influence near the wall. With the DNS in the transitional regime, the near-wall flow will be affected only to a small degree by viscous drag, resulting in a strongly reduced peak value. The small peak very close to the wall is caused by a region of local separation right above the roughness element. The $\overline{u^{+2}}$ profile also suggests that the roughness effect is quite local, extending only out to $y/h \approx 0.2$, which corresponds to about 6 roughness heights. These data therefore seem to support the 'wall similarity' hypothesis.

The surface roughness is also expected to severely affect the wall normal stress, $\overline{v^{+2}}$, due to the reduced damping effect near the wall. Krogstad & Antonia (1999) claim that the effect depends strongly on the wall geometry, suggesting that two-dimensional roughnesses such as spanwise rods have a much stronger effect on $\overline{v^{+2}}$ than a random three-dimensional geometry. In their investigation of a boundary layer with rod roughness, it was found that $\overline{v^{+2}}$ was strongly reduced near the wall, but they also observed a significant increase in the outer layer. In the present experimental data a reduction in $\overline{v^{+2}}$ up to $y/h \approx 0.2$ is observed in the measurements and the effect appears to extend even further out in the DNS (figure 5). The increased level of the smooth wall $\overline{v^{+2}}$ for the experiments compared to the DNS for $y/h < 0.1$ is due to problems of the hot wire measuring v correctly near the wall. However, in the outer layer the similarity in the experimental data is very good and a small decrease is found in the DNS data. Hence a possible increase in $\overline{v^{+2}}$ in the outer layer appears

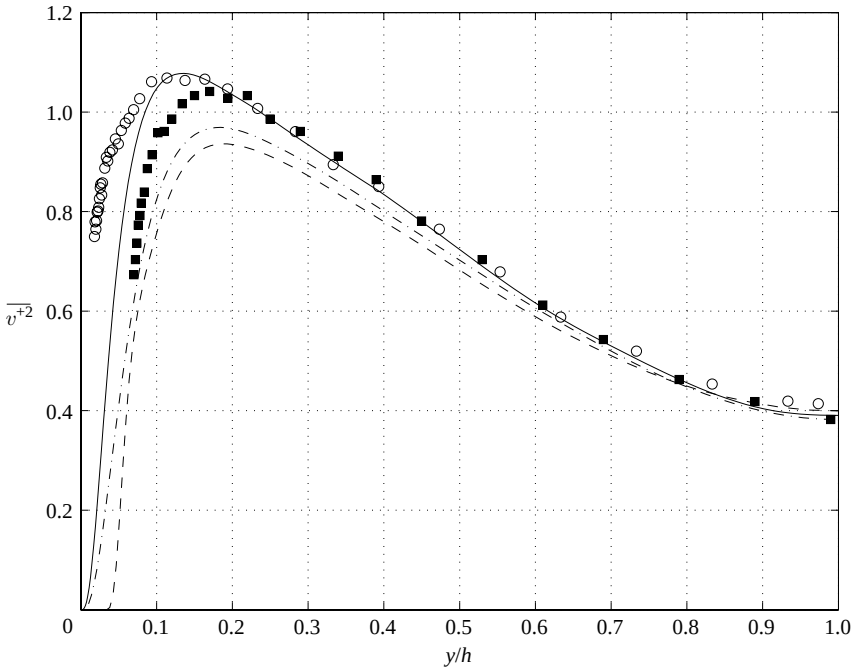

FIGURE 5. Wall-normal stress profiles, $\overline{v^{+2}}$. Symbols as in figure 2.

to be a phenomenon that is unique to boundary layers and is not verified for the channel flow. It should also be mentioned that the rough wall channel flow DNS of Miyake *et al.* (2000) ($Re_\tau = 150$) indicates that $\overline{v^{+2}}$ is virtually unaffected by the roughness throughout the layer.

The spanwise normal stress, $\overline{w^{+2}}$, is shown in figure 6. This stress is clearly overestimated close to the wall in the experiment compared to the DNS. This is a well-known phenomenon when using a probe configuration with one wire on top of the other. The effect of the roughness seems to be very small and is only apparent as a small dip and peak in the experimental data right above the roughness element. This trend is also evident in the DNS. Further out the collapse of both the experimental and DNS data is very good.

Again, the available DNS do not appear to give a unique trend. The DNS of Leonardi *et al.* (2004) indicates a substantial increase in the plane-averaged $\overline{w^{+2}}$ above the plane of the ribs. The increase in peak value for the geometry used in that investigation was of the order of 20%. This is significantly higher than what is found in the present DNS. (However, as noted in § 1, their k/h ratio is much higher than the criterion of Jimenez 2004). The DNS of Miyake *et al.* (2000), however, indicates a reduction of about 7% in the peak value of $\overline{w^{+2}}$ for sand grain roughness.

The shear stress profiles above the crests of the roughness elements are shown in figure 7. As expected, the data collapse onto a straight line in the outer layer irrespective of the surface condition, consistent with (2.5). Due to the increased turbulence intensity over the rough surface, the peak in the measured $-\overline{u^+v^+}$ is likely to be underestimated in the rough case. This explains why the roughness effect appears to extend further out from the wall in the experiment than in the DNS.

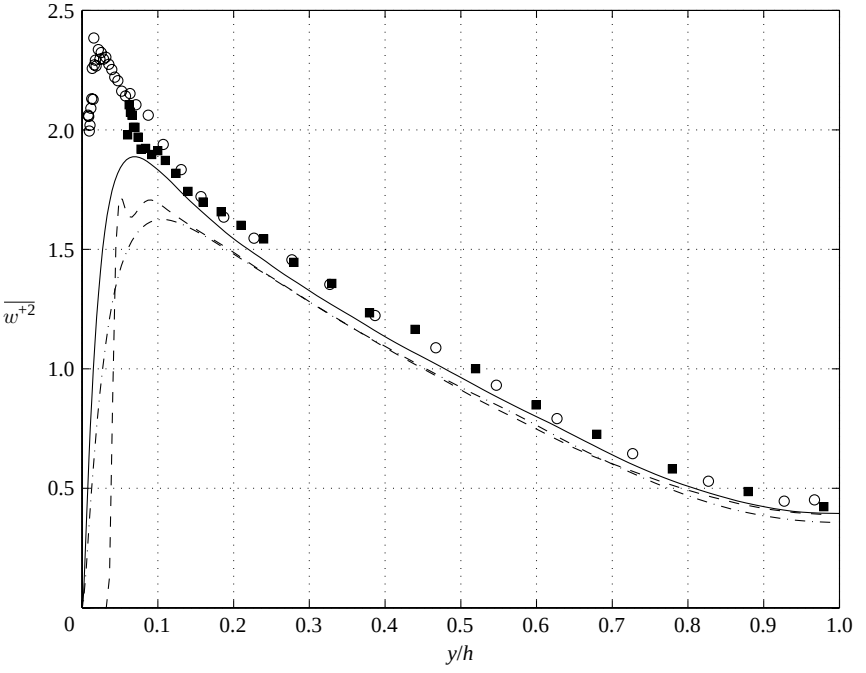

FIGURE 6. Spanwise stress profiles, $\overline{w^{+2}}$. Symbols as in figure 2.

6. Roughness effects on the turbulent structure

In order to study the structural effects of the surface roughness on the flow in more detail, a quadrant analysis and a study of the anisotropy tensor are undertaken. These methods were chosen since they are equally well adapted to analyse experimental and DNS data. The quadrant analysis is capable of providing information about changes in the turbulent flow pattern due to the modified wall boundary condition, while the anisotropy analysis will give information about how the interaction between the stresses in the flow may have been affected.

6.1. *Quadrant analysis*

Quadrant analysis has proven to be a convenient tool to extract information about changes in turbulent structure when comparing turbulent flows. By sorting the turbulent events into the various quadrants of the (u, v)-plane, statistical information about the flow patterns may be educed. The most important events are the ejections ($Q2$) and sweeps ($Q4$) which are events occurring in the second and fourth quadrants respectively. For smooth wall flows, the ejection events draw fluid from the low-speed streaky structures embedded in the viscous sublayer and transport it to the outer layer. Even though the streaks must be considerably modified by the roughness elements, the flow visualizations of Grass (1971) for gravel type surface roughness clearly show the existence of ejections and sweeps previously identified with the smooth wall 'bursting process' in the rough wall case also. Grass noted that over rough walls the ejections could be very violent, with ejected fluid "rising almost vertically from the interstices between the roughness elements". He also observed that the ejections were often coherent over much of the layer. In contrast, sweep motions were confined to the region close to the wall. Hence it appears that much of the mixing properties in a turbulent wall flow should be independent of the surface condition.

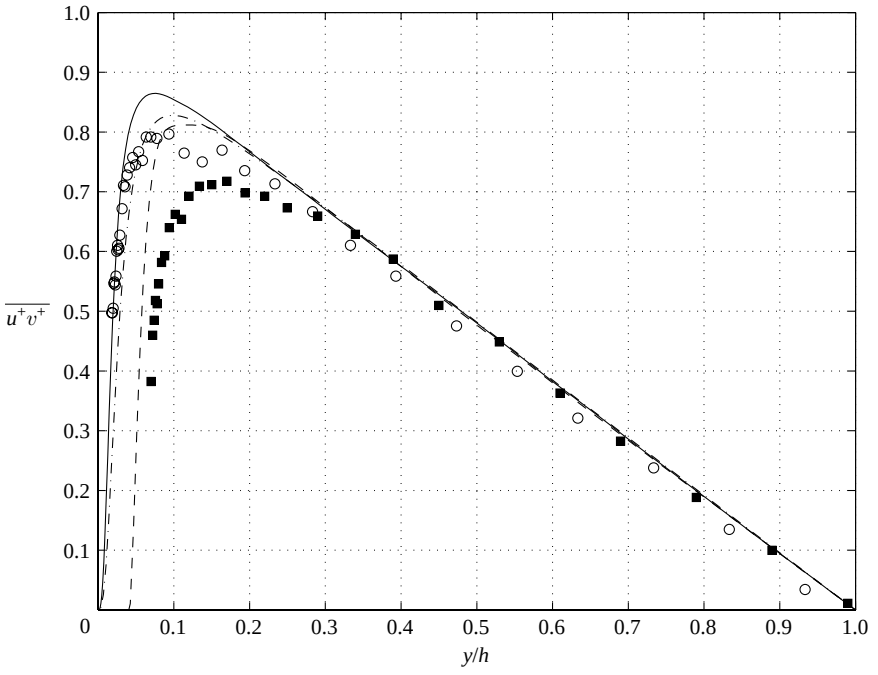

FIGURE 7. Shear stress profiles, $-\overline{u^+v^+}$. Symbols as in figure 2.

The u, v quadrant decomposition technique has been effective for assessing the importance of the visually observed ejections and sweeps in the wall region. Here we will use the technique to further elucidate the region directly affected by the roughness elements. Using Lu & Willmarth's (1973) concept of a hyperbolic hole of size H, defined by $| uv | = Hu'v'$ (a prime denotes an r.m.s. value), the contribution to $\overline{uv}$ from a particular quadrant can be written as

$$(\overline{uv})_Q = \lim_{T\to\infty} \frac{1}{T} \int_0^T uv\, I(t)\, \mathrm{d}t, \tag{6.1}$$

where I_2 is an indicator function defined so that

$$I(t) = \begin{cases} 1 & \text{when } | uv |_Q \geqslant Hu'v' \\ 0 & \text{otherwise.} \end{cases}$$

Here the velocity vector used to compute $(\overline{uv})_Q$ is assumed to be a function of time only, as will be the case for the signals from a hot-wire probe.

For a DNS database the velocity vectors are available as a spatially distributed function for a limited number, N_t, of realizations separated in time. Assuming that the turbulent quantities are periodic in the streamwise direction and homogeneous in the spanwise direction, the quadrant decomposition for the DNS data base may be written

$$(\overline{uv})_Q = \frac{1}{N_t\, N_{sp}\, N_{per}} \sum_{i=1}^{N_t} \sum_{j=1}^{N_{sp}} \sum_{k=1}^{N_{per}} uv I_{i,j,k}, \tag{6.2}$$

where N_{sp} is the number of grid points in the spanwise direction and N_{per} is the number of periodic elements in the simulation domain. $I_{i,j,k}$ has the same definition as in the temporal case.

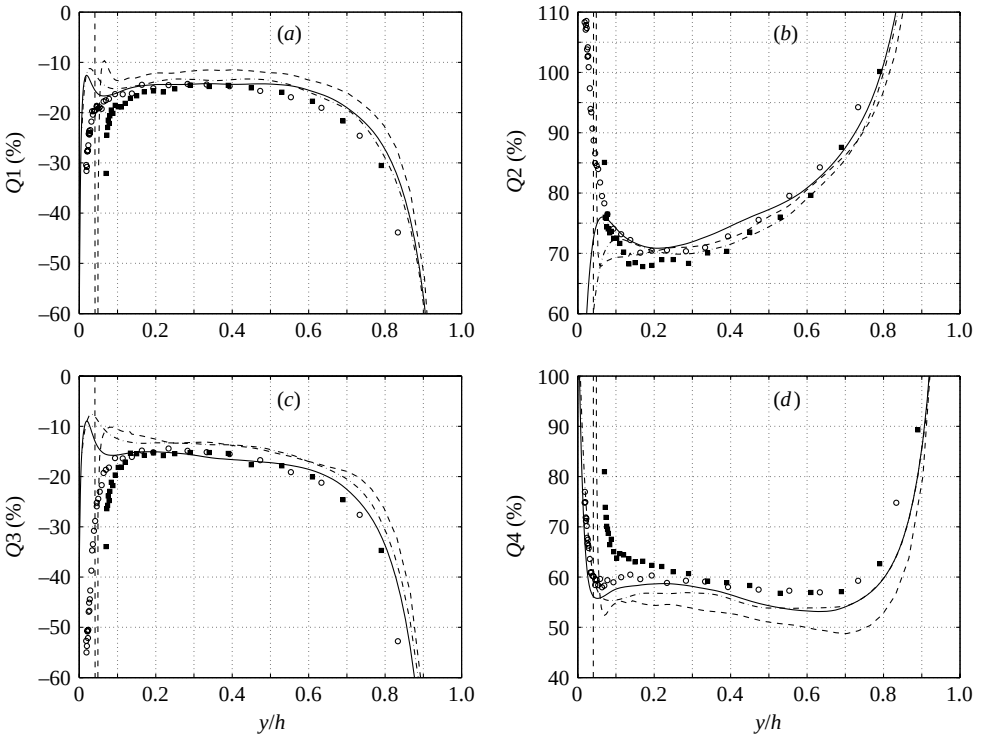

FIGURE 8. Contributions to the quadrants: $H = 0$. (*a*) $Q1$, (*b*) $Q2$, (*c*) $Q3$, (*d*) $Q4$. Symbols as in figure 2.

In general, it is difficult to compare structural information between DNS and hot-wire data, since the spatial averaging performed using (6.2) in the case of DNS will be different from the temporal averaged data obtained from the hot wire using (6.1). However, when $H = 0$, the two processes will be equivalent, since all data will be used in both cases. Hence, a quadrant analysis comparison between the DNS and experimental data will be shown for $H = 0$ only. (The data will be presented as the percentage contribution to $\overline{uv}$ from each quadrant, i.e. as $F_Q = 100\% \times (\overline{uv})_Q/\overline{uv}$, since this does not carry any inaccuracy in the selection of a scaling variable, such as u_τ etc.)

The percentage contributions to $-\overline{uv}$ from $Q1$ measured above the crest of the roughness elements are shown in figure 8(*a*). The contribution is always negative, since $\overline{uv}$ is negative in the measurement region. As expected from the shear stress profiles, the smooth wall experimental data follow the DNS distribution well, except very close to the surface, where the hot-wire data fail to pick up the small peak. As discussed previously, this is due to problems of the hot wire measuring v correctly near the wall.

The measured rough wall distribution follows that of the smooth wall very well in the outer layer. Right above the roughness elements a shift in the distribution away from the wall of about 1 to 2 roughness heights is observed. The roughness effects are more pronounced in the DNS, where a general reduction in the outer layer is also found. Comparing figure 8(*a*) to figures 4 and 5, it is evident that this reduction is linked to the much stronger reduction in $\overline{v^{+2}}$ picked up by the DNS than in the experiment. The smooth wall minimum near $y/h \approx 0.03$ is maintained in the rough wall DNS, but shifted outwards 1 to 2 roughness heights. The quadrant analysis

results from the DNS of Leonardi (2002) show the same outward shift of the near-wall peak and a reduction further out, corroborating the present DNS results. His results suggest a peak contribution right above the roughness element of 140%, which is significantly stronger than the value found here.

The distributions for the more important ejection events ($Q2$) are shown in figure 8(b). The outer layer is very little affected by the roughness, but a distinct near-wall reduction in $Q2$ activities is evident both in the DNS and the experimental data. Both investigations suggest an effect out to $y/h \approx 0.2$, corresponding to about 6 times the height of the roughness elements. The local peak in $Q2$ observed in the DNS for the smooth wall is reduced to a local minimum in the rough case. This near-wall reduction is in agreement with the findings of Krogstad & Antonia (1999), who found that the $Q2$ contributions for strong events ($H = 2.5$) virtually vanished. Hence, it appears that the 'very violent' ejection events observed by Grass (1971) produce very little shear stress. This reduction is explained by Grass as low-momentum fluid being trapped between the roughness elements. However, both the measurements and DNS are at variance with the results of Leonardi (2002), who found a general increase in contributions to $-\overline{uv}$ from $Q2$ throughout the channel.

Figure 8(c) shows the roughness effects on $Q3$, frequently denoted the 'inward interaction' quadrant. The trends are the same as observed for $Q1$. Except for a general reduction in contributions found in the DNS, which is not picked up in the measurements, the roughness effects are very local. Again our results are not in agreement with those of Leonardi (2002), who found a general increase in $Q3$ contributions across the channel.

The roughness effects on the sweep events ($Q4$) are not clear from the present results (figure 8d). The DNS data suggest a general reduction throughout most of the layer, and only a small outward shift near the wall. This is supported by the DNS of Leonardi (2002). The near-wall peak above the roughness element found in his simulation is almost doubled compared to the smooth case, a result which is not supported by the present results. In contrast to this the measurements show no outer layer effects but a significant increase for $y/h < 0.3$. The experimental observation is consistent with most measurement results available (e.g. Krogstad & Antonia 1999; Raupach *et al.* 1991). However, the general conclusion drawn from figure 8(a)–(d) is that the surface roughness impact on the outer layer turbulent structure is likely to be stronger than suggested by a direct inspection of the stresses alone.

Because of the general diffusion of turbulent energy from the wall region to the outer layer, $Q2$ must be the dominant quadrant. The contributions from this quadrant are closely balanced by the contributions from $Q4$. Figure 9(a) shows the ratios between the contributions from these two quadrants. To highlight the distributions near the wall, the same ratio is plotted in semi-logarithmic scales in figure 9(b). In the smooth cases the near-wall Re_τ effects are evident and it is apparent that the measurements overestimate the importance of $Q2$, as expected from the measured $\overline{v^{+2}}$ profile. In the rough wall case the ratio drops close to 1 while the DNS remains about 20% higher throughout most of the flow region. This increase has been verified in the DNS of Leonardi (2002) and Nakagawa, Na & Hanratty (2003). The simulations of Leonardi (2002) also indicate a rapid drop down to $Q2/Q4 \approx 0.7$ near the top of the roughness elements.

6.2. *Reynolds stress anisotropy*

There seems to be a general agreement that the surface roughness affects the turbulent structure near the wall. However, outside the roughness sublayer, there is apparently

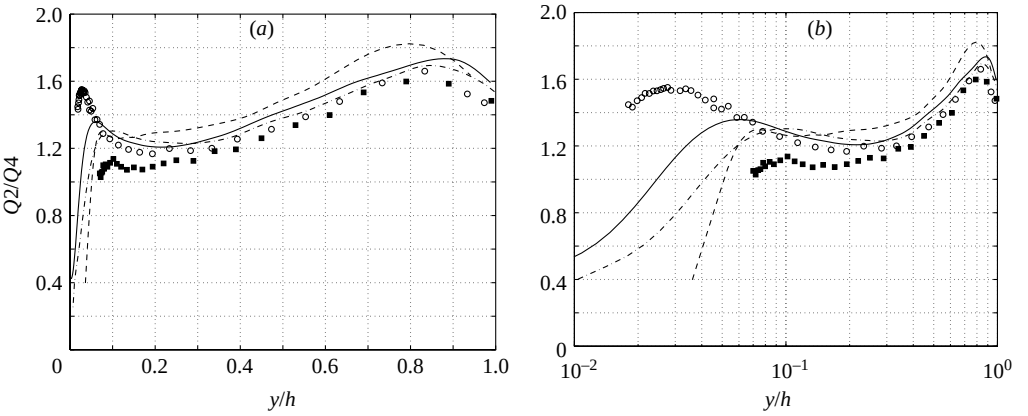

FIGURE 9. $Q2/Q4$ ratios: $H = 0$. (*a*) outer variables, (*b*) inner variables. Symbols as in figure 2.

little consensus on this topic. The classical theory that the turbulence structure is little affected by the roughness in the outer layer receives support in a boundary layer from Grass (1971) and Raupach *et al.* (1991). This conjecture is also corroborated for the channel flow by the recent DNS of Miyake *et al.* (2000) and the particle image velocimetry measurements of Nakagawa & Hanratty (2001). The structure functions measured by Poggi *et al.* (2003) above a mesh surface in an open channel flow confirm these findings. Ligrani & Moffat (1986) showed that there was very little variation in the shear stress correlation coefficient, $\rho_{uv} = -\overline{uv}/(\overline{u^2}\ \overline{v^2})^{1/2}$, from transitionally to fully rough boundary layer flow, indicating that the type of mechanism resulting in the production of turbulence does not change with surface roughness. In contrast to these findings, Krogstad & Antonia (1994) claimed that roughness tends to reduce the overall anisotropy of the large-scale motion in a boundary layer with *k*-type rod roughness. This was supported by the measurements of the anisotropy tensor of Shafi & Antonia (1995) for a mesh surface and Keirsbulck *et al.* (2002) for a rod-type roughness in a boundary layer. Djenidi, Elavarasan & Antonia (1999) investigated a boundary layer with *d*-type square rod roughness. They found that the anisotropy invariants had a smaller tendency towards isotropy than the mesh surface of Shafi & Antonia (1995), indicating that the 'interaction' between the wall and the outer layer may be controlled by the wall geometry. As opposed to these findings, Mazouz, Labraga & Tournier (1988) (channel) and Sabot, Saleh & Comte-Bellot (1977) (pipe) found that the anisotropy with *k*-type rod roughness was increased by the roughness, suggesting that the flow type was important. It must be noted that in both of the latter studies the roughness elements were larger than what was suggested by Jimenez (2004) to be the limit for the roughness elements to not directly affect the outer flow. The evidence from experiments and simulations is not very conclusive, and the result so far in the present study is that the roughness effect is limited to the very near-wall region. It is therefore of interest to investigate the influence of roughness on the anisotropy in the outer layer in the present channel flow.

A rough guide to the large-scale anisotropy may be obtained by studying the ratios between the various Reynolds stresses. If the flow becomes more isotropic when surface roughness is added, the stress ratio $\overline{v^2}/\overline{u^2}$ (figure 10*a*) is expected to increase as $\overline{v^{+2}}$ is increased and $\overline{u^{+2}}$ reduced. This is the case neither in the experiment nor in the DNS. Except for a shift near the wall due to Re_τ effects, the two cases indicate

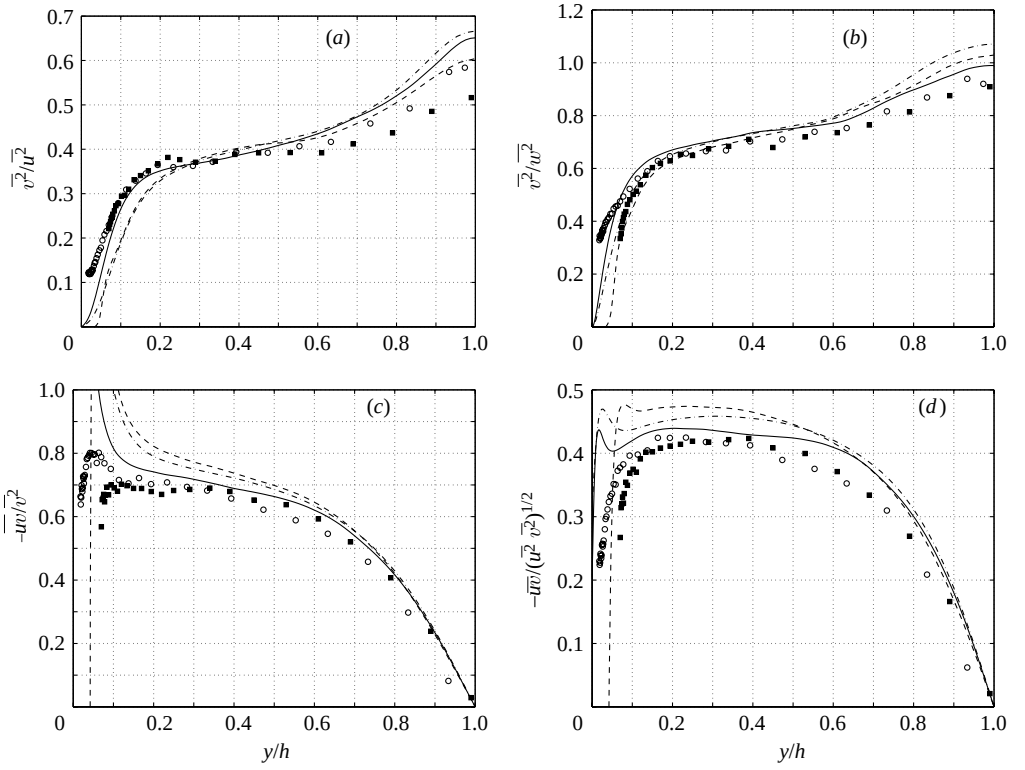

FIGURE 10. Stress ratios: (*a*) $\overline{v^2}/\overline{u^2}$, (*b*) $\overline{v^2}/\overline{w^2}$, (*c*) $\overline{uv}/\overline{v^2}$, (*d*) $\rho_{uv} = -\overline{uv}(\overline{u^2}\,\overline{v^2})^{1/2}$. Symbols as in figure 2.

that the stress ratio is the same for both surfaces over the entire width of the channel. (The reason for the small discrepancies in the outer layer both in the DNS and the measurements is so far unclear. It is not believed to be a roughness effect, since it is hard to imagine a change in the outer layer without a significant difference near the wall also.)

The similarity in stress ratio means that the reduction observed in $\overline{u^{+2}}$ in the inner part of the flow in the rough wall channel (figure 4) is accompanied by a proportional reduction in $\overline{v^{+2}}$ (figure 5). Some differences are found in the other stress ratios in the wall region however. For the flow to be more isotropic an increase in $\overline{v^2}/\overline{w^2}$ towards unity would be expected, but instead a small reduction is observed near the wall (figure 10*b*), in agreement with the observation in figure 6 that the spanwise stress $\overline{w^{+2}}$ is very little affected by the wall roughness.

A reduced anisotropy would also imply that the ratio $-\overline{uv}/\overline{v^2}$ must be reduced as $-\overline{u^+v^+}$ has to tend towards zero and $\overline{v^{2^+}}$ ought to increase. For the experiments, figure 10(*c*) shows that $-\overline{uv}/\overline{v^2}$ is reduced near the wall in the rough case and that this effect extends out to about $y/h \approx 0.1$. From the observations about the other stress ratios it is apparent that the reduction in $-\overline{uv}/\overline{v^2}$ is mainly due to a reduction in $-\overline{u^+v^+}$. The DNS results tend to infinity near the wall, because $\overline{v^2}$ approaches zero faster than $-\overline{uv}$. The two quantities $-\overline{uv}$ and $\overline{v^2}$ are measures of the 'active motion', hence also the ratio $-\overline{uv}/\overline{v^2}$. An implication of figure 10(*c*) is that the 'active' motion is *Re*-dependent at low Re_τ. This is consistent with the findings of Antonia *et al.* (1992) and Bakken & Krogstad (2005). As opposed to this result, the ratio between

the 'active' component $\overline{v^2}$ and the 'inactive' component $\overline{w^2}$ (figure 10*b*) seems to be less affected by Re_τ.

The correlation coefficient, ρ_{uv}, is shown in figure 10(*d*). A wide region with a value slightly higher than 0.4 is observed and corresponds well with earlier reported results. A reduction in ρ_{uv} near the rough surface indicates that the anisotropy is reduced. Outside the roughness sublayer, i.e. for $0.05 < y/h < 0.4$, the DNS data indicate a tendency towards slightly lower anisotropy over the rough wall whereas the experiments display a high degree of similarity in this region. This discrepancy is probably caused by the difference in $\overline{v^{+2}}$ discussed in the previous section. However, the most apparent property of figures 10(*c*) and 10(*d*) is the Reynolds number dependence in the central region of the profiles.

Since the stress ratios do not give conclusive information about the claimed tendency for the flow to become more isotropic over a rough surface, a more accurate measure for anisotropy must be used. The anisotropy tensor

$$b_{ij} = \frac{\overline{u_i u_j}}{\overline{u_\ell u_\ell}} - \frac{\delta_{ij}}{3} \tag{6.3}$$

was therefore computed for the two flows, where repeated indices means summation and δ_{ij} is the Kronecker delta function.

Two of the criteria for approximate self-similarity in the log-law region are that the production balances the dissipation, $P_k/\epsilon \approx 1$, and that the components of b_{ij} are essentially uniform. For the DNS data of Moser *et al.* (1999), $P_k/\epsilon = 1 \pm 0.15$ for $0.05 < y/h < 0.6$. Ashrafian & Andersson (2004) have shown that this is also valid for the rod roughness for $5k < y < 0.6h$. The parameter $-b_{12}$ is often referred to as the Townsend structure parameter, a_1 (Townsend 1961). In two-equation models based on the eddy viscosity, ν_τ, this parameter is assumed to be constant and equal to 0.15 in the logarithmic layer, which leads to the value of 0.09 for C_μ, where $\nu_\tau = C_\mu \overline{u_\ell u_\ell}/\epsilon$. This assumption is valid for layers of approximate self-similarity.

The data for b_{ij} are plotted in figure 11. Inside $y \approx 5k$, both the measurements and DNS indicate that for the rough wall flow, all stresses except $\overline{v^2}$ are closer to isotropy than in the smooth case (see b_{22}). The effect is strongest for b_{33} (i.e. for $\overline{w^2}$) where the strong near-wall peak is removed. For the other components, the effect is small, although a fairly strong reduction right at the top of the rib is evident for b_{11} and $-b_{12}$. The measured normal components are generally lower than those estimated from DNS in the wall region, reflecting the inaccuracy in the measured stress components.

In the outer layer, the collapse between the smooth and rough surface data is very good both for the DNS and the experiments. The differences between the simulations and the measurements are generally small. For all the normal stresses, there is a small, but discernible Reynolds number dependence in the outer layer, leading to a corresponding dependence in the turbulent kinetic energy (not shown). For the $-b_{12}$ component the experimental data are somewhat more isotropic than the DNS. This is believed to be a Reynolds number effect caused by the increase in the turbulent kinetic energy with increasing Re_τ. The $-b_{12}$ component is the most affected, since $-\overline{u^+v^+}$ is the only stress component which must be unaffected by Re_τ in the outer region. This conjecture is also supported by the more isotropic $Re_\tau = 590$ smooth wall DNS data compared to the results from the present $Re_\tau = 400$ smooth wall DNS. In the central part of the profiles all the components of b_{ij} are reasonably constant, indicating a region of approximate self-similarity. The value of $-b_{12}$ is 0.14 ± 0.01 for $5k < y < 0.6h$, which corresponds well with the assumption made for the two-equation

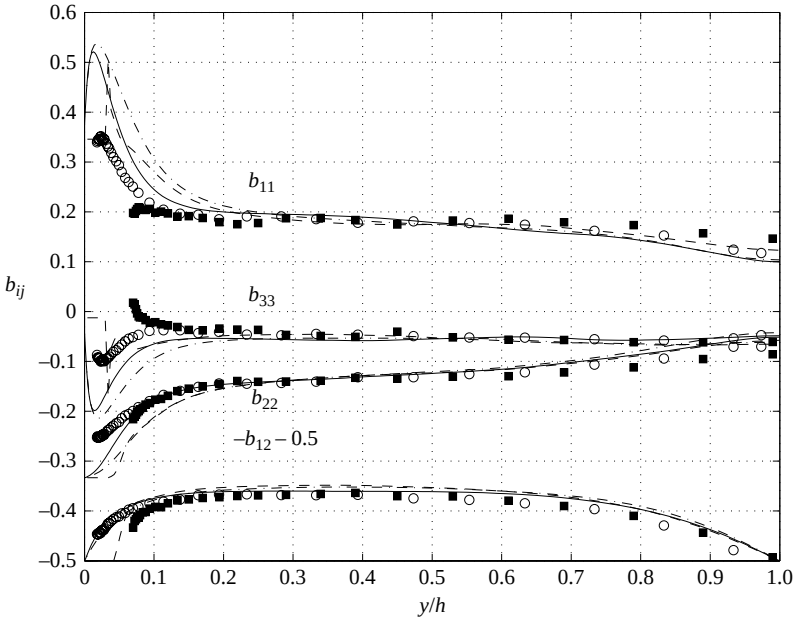

FIGURE 11. The non-zero elements of the anisotropy tensor b_{ij}. Note that $-b_{12}$ is shifted downwards by 0.5 to avoid crowding. Symbols as in figure 2.

models. At the centreline, the shear stress vanishes, so $-b_{12}$ is naturally zero. The other components are still anisotropic, although less so than in the region of approximate self-similarity.

Lumley & Newman (1976) suggested the function $F = 1 + 9II + 27III$ as an estimate of the overall anisotropy of the Reynolds stress tensor in the flow, where $II = \frac{1}{2}b_{ij}b_{ji} = b_{11}^2 - b_{22}b_{33} + b_{12}^2$ and $III = \frac{1}{3}b_{ij}b_{jk}b_{ki} = b_{33}(b_{11}\,b_{22} - b_{12}^2)$ for a two-dimensional channel flow. The range limits of F are the two-component turbulence value $F = 0$ and the three-component isotropic condition $F = 1$. Figure 12 shows that there is a clear Reynolds number dependence near the wall, resulting in a more isotropic flow with increasing Re_τ. The region of constant F corresponds to the range of approximate self-similarity, indicating that the log-region is a region of constant anisotropy. There is a clear approach towards isotropy near the centreline.

The present results deviate substantially from the boundary layer and channel flow data compiled by Smalley *et al.* (2002), who compared the mesh surface boundary layer data of Shafi & Antonia (1995), rod roughness data of Antonia & Krogstad (2001) and the perforated plate roughness of Saddoughi & Veeravalli (1994) with the smooth wall data of Spalart (1988) (DNS), Erm & Joubert (1991) and Smith (1994). They found that in the outer layer ($y/\delta > 0.1$, where y is measured from the top of the roughness element) b_{11} and b_{22} were generally smaller in magnitude for rough walls than over smooth surfaces, indicating a tendency for the rough walls to reduce anisotropy. Only for rod roughness was there also a reduction in b_{33}. This conclusion is not supported by the present rod roughness data, where neither b_{11} nor b_{22} nor b_{33} show any roughness influence in the outer layer. For the channel flow DNS data with rod roughness on one side and varying pitch ratio (Leonardi 2002), a general reduction in anisotropy was observed over the rough surfaces and the reduction was markedly stronger for the k-type than for the d-type roughness. As noted in § 1, the latter data were obtained using fairly large roughness elements ($k/h = 0.1$).

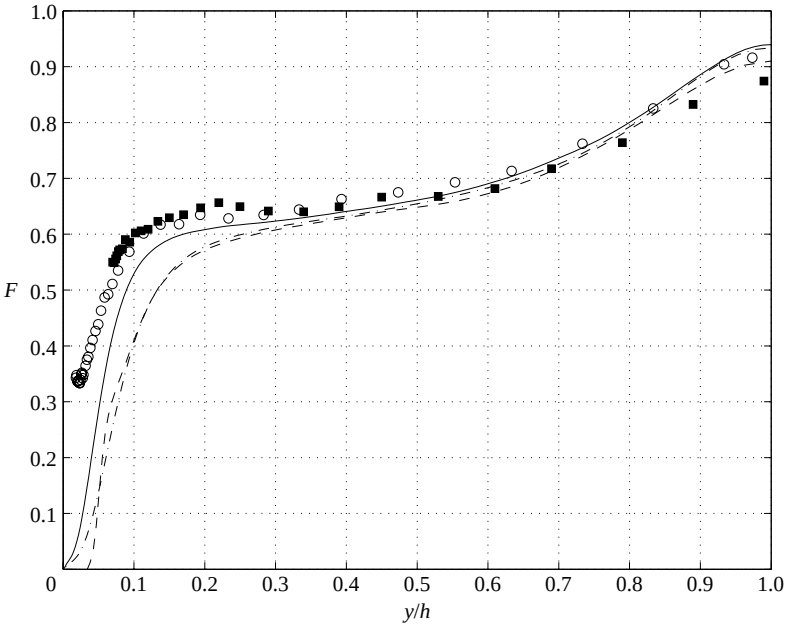

FIGURE 12. Invariant function $F = 1 + 9II + 27III$. Symbols as in figure 2.

There seems to be ample evidence for the anisotropy to be dependent on the flow type. A large majority of the boundary layer data support the theory of the anisotropy being dependent on the specific type of roughness for a major part of the flow. The present study is clearly challenging this conjecture for internal flows, displaying a high degree of similarity between the smooth and rough surfaces.

7. Conclusions

Data from a rod-roughened turbulent channel flow have been compared with corresponding data over a smooth surface using hot-wire anemometry and DNS. The Reynolds number of the DNS is in the top end of the transitional regime, whereas that of the experiment is in the fully rough regime. There seem to be three effects of this difference in flow regime. First, the total flow resistance for the DNS is somewhat influenced by viscous shear whereas only pressure-induced form drag is important for the experiments. The value of the friction factor for the DNS is therefore slightly lower than for the experiment. Secondly, the effect of the roughness on the mean velocity profile, as measured by ΔU^+, is less pronounced for the DNS than what would be expected from the fully rough experimental results. The third effect is a higher near-wall peak value of $\overline{u^{+2}}$ for the rough wall DNS than for the experiment. This is due to a high degree of coherence in the structures near the boundary in a smooth wall case, causing a high peak value for $\overline{u^{+2}}$, whereas the break-up of these structures by the roughness causes the peak value to decrease with increasing k^+.

The similarity in the velocity defect plot suggests that there is no influence of surface roughness in the outer region. For the Reynolds stresses, only the DNS results of $\overline{v^{+2}}$ display differences outside $y \approx 5k$. However, the rough wall profile is attenuated in the outer region, which is the opposite of what has been observed for a boundary layer.

The turbulence structure seems to be somewhat more affected in the outer region than suggested by the stresses. The results from a quadrant analysis show that the ejections are weaker right above the roughness, probably due to low-momentum fluid being trapped between the roughness elements. The results on the sweep type events are somewhat ambiguous, but the experimental data support the general view that sweeps are enhanced near a rough surface due to the reduced damping of the wall-normal motion. The results from the anisotropy tensor support the notion of a more isotropic flow near a rough surface. However, as opposed to recent boundary layer results, the outer layer seems to be very little affected by the roughness.

The results from the present investigation generally support the wall similarity hypothesis of Townsend (1976) for a channel flow. In the light of the many recent investigations on rough wall boundary layers suggesting the opposite, it is speculated that surface roughness effects on the outer layer may be dependent on flow type.

This work has been supported by The Research Council of Norway through a grant of computing time (Programme for Supercomputing) and a research fellowship to A. A. under contract no. 134939/432. The computer code MGLET was kindly made available by Professor R. Friedrich (TU München) and Professor H. Wengle (Universität Bundeswehr München). Numerous discussions with Dr S. Leonardi (University of Rome "La Sapienza) and Dr M. Manhart (TU München) are gratefully acknowledged.

REFERENCES

Abe, H., Kawamura, H. & Matsuo, Y. 2001 Direct numerical simulation of a fully developed turbulent channel flow with respect to the Reynolds number dependence. *Trans. ASME*: *J. Fluids Engng* **123**, 382–393.

Andreopoulos, J. & Bradshaw, P. 1981 Measurements of turbulence structure in the boundary layer on a rough surface. *Boundary-Layer Met.* **20**, 201–213.

Antonia, R. A. & Krogstad, P.-Å. 2001 Turbulence structure in boundary layers over different types of surface roughness. *Fluid Dyn. Res.* **28**, 139–157.

Antonia, R. A., Teitel, M., Kim, J. & Browne, L. W. B. 1992 Low-Reynolds-number effects in a fully developed turbulent channel flow. *J. Fluid Mech.* **236**, 579–605

Ashrafian, A. & Andersson, H. I. 2004 Roughness effects in turbulent channel flow. *Intl J. Prog. Comput. Fluid Dyn.* (submitted).

Ashrafian, A., Andersson, H. I. & Manhart, M. 2004 DNS of turbulent flow in a rod-roughened channel. *Intl J. Heat Fluid Flow* **25**, 373–383.

Bakken, O. M. & Krogstad, P.-Å. 2004 A velocity dependent effective angle method for calibration of X-probes at low velocities. *Exps. Fluids* **37**, 146–152.

Bakken, O. M. & Krogstad, P.-Å. 2005 Reynolds number effects in the outer layer of the turbulent flow in a channel with rough walls. *Phys. Fluids* (in press).

Bearman, P. W. 1971 Corrections for the effect of ambient temperature drift on hot-wire measurements in incompressible flow. *DISA Info.* **11**, 25–30.

Chorin, A. J. 1968 Numerical solution of the Navier–Stokes equations. *Math. Comput.* **22**, 745–762.

Cui, J., Patel, V. C. & Lin, C.-L. 2003 Large-eddy simulation of turbulent flow in a channel with rib roughness. *Intl. J. Heat Fluid Flow* **24**, 372–388.

Djenidi, L., Elavarasan, R. & Antonia, R. A. 1999 The turbulent boundary layer over transverse square cavities. *J. Fluid Mech.* **395**, 271–294.

Erm, L. P. & Joubert, P. N. 1991 Low-Reynolds number turbulent boundary layer. *J. Fluid Mech.* **230**, 1–44.

Furuya, Y., Miyata, M. & Fujita, H. 1976 Turbulent boundary layer and flow resistance on plates roughened by wires. *Trans. ASME*: *J. Fluids Engng* **98**, 635–644.

Grass, A. J. 1971 Structural features of turbulent flow over smooth and rough boundaries. *J. Fluid Mech.* **50**, 233–255.

Grötzbach, G. 1983 Spatial resolution requirements for direct numerical simulation of the Rayleigh–Bénard convection. *J. Comput. Phys.* **49**, 241–264.

Hanjalic, K. & Launder, B. E. 1972 Fully developed asymmetric flow in a plane channel. *J. Fluid Mech.* **51**, 301–335.

Hirt, C. W., Nichols, B. D. & Romero, N. C. 1975 SOLA – A numerical solution algorithm for transient fluid flows. *Los Alamos Sci. Lab. Rep.* Los Alamos.

Ikeda, T. & Durbin, P. A. 2002 Direct simulations of a rough-wall channel flow. *Rep.* TF-81. Dept. Mech. Eng., Stanford University.

Jimenez, J. 2004 Turbulent flows over rough walls. *Annu. Rev. Fluid Mech.* **36**, 173–196.

Jimenez, J. & Moin, P. 1991 The minimal flow unit in near wall turbulence. *J. Fluid Mech.* **225**, 221–240.

Johansson, P. S. & Andersson, H. I. 2004 Generation of inflow data for inhomogeneous turbulence. *Theor. Comput. Fluid Dyn.* **18**, 371–389.

Keirsbulck, L., Labraga, L., Mazouz, A. & Tournier, C. 2002 Influence of surface roughness on anisotropy in a turbulent boundary layer flow. *Exps. Fluids* **33**, 497–499.

Kline, S. J., Reynolds, W. C., Schraub, F. A. & Rundstadler, P. W. 1967 The structure of turbulent boundary layers. *J. Fluid Mech.* **30**, 741–773.

Krogstad, P.-Å. & Antonia, R. A. 1994 Structure of turbulent boundary layers on smooth and rough walls. *J. Fluid Mech.* **277**, 1–21.

Krogstad, P.-Å. & Antonia, R. A. 1999 Surface roughness effects in turbulent boundary layers. *Exps. Fluids* **27**, 450–460.

Krogstad, P.-Å., Antonia, R. A. & Browne, L. W. B. 1992 Comparison between rough- and smooth-wall turbulent boundary layers. *J. Fluid Mech.* **245**, 599–617.

Lee, C. 2002 Large-eddy simulation of rough-wall turbulent boundary layers. *AIAA J.* **40**, 2127–2130.

Leonardi, S. 2002 Turbulent channel flow with roughness: direct numerical simulations. PhD Thesis, Universita di Roma "La Sapienza".

Leonardi, S., Orlandi, P., Djenidi, L. & Antonia, R. A. 2004 Structure of turbulent channel flow with square bars on one wall. *Intl J. Heat Fluid Flow* **25**, 384–392.

Leonardi, S., Orlandi, P., Smalley, R. J., Djenidi, L. & Antonia, R. A. 2003 Direct numerical simulation of turbulent channel flow with transverse square bars on one wall. *J. Fluid Mech.* **491**, 229–238.

Ligrani, P. M. & Moffat, R. J. 1986 Structure of transitionally rough and fully rough turbulent boundary layers. *J. Fluid Mech.* **162**, 69–98

Lu, S. S. & Willmarth, W. W. 1973 Measurements of the structure of the Reynolds stress in a turbulent boundary layer. *J. Fluid Mech.* **60**, 481–571.

Lumley, J. L. & Newman, G. R. 1976 The return to isotropy of homogeneous turbulence. *J. Fluid Mech.* **82**, 161–178.

Mazouz, A., Labraga, L. & Tournier, C. 1998 Anisotropy invariants of Reynolds stress tensor in a duct flow and turbulent boundary layer. *Trans. ASME: J. Fluids Engng* **120**, 280–284.

Miyake, Y., Tsujimoto, K. & Agata, Y. 2000 A DNS of a turbulent flow in a rough-wall channel using roughness elements model. *JSME Intl J.* B **43** (8), 233–242.

Miayke, Y., Tsujimoto, K. & Masaru, N. 2001 Direct numerical simulation of rough-wall heat transfer in a turbulent channel flow. *Intl J. Heat Fluid Flow* **22**, 237–244.

Moser, R. D., Kim, J. & Mansour, N. N. 1999 Direct numerical simulation of turbulent channel flow up to $Re_\tau = 590$. *Phys. Fluids* **11**, 943–945.

Nagano, Y., Hattori, H. & Houra, T. 2004 DNS of velocity and thermal fields in turbulent channel flow with transverse-rib roughness. *Intl J. Heat Fluid Flow* **25**, 393–403.

Nakagawa, S. & Hanratty, T. J. 2001 Particle image velocimetry of flow over a wavy wall. *Phys. Fluids* **13**, 3504–3507.

Nakagawa, S., Na, Y. & Hanratty, T. J. 2003 Influence on a wavy boundary in turbulence. I. Highly rough surface. *Exps. Fluids* **35**, 422–436.

Orellano, A. & Wengle, H. 2000 Numerical simulation(DNS and LES) of manipulated turbulent boundary layer flow over a surface-mounted fence. *Eur. J. Mech.* B **19**, 765–788.

Poggi, D., Porporato, A. & Ridolfi, L. 2003 Analysis of the small-scale structure of turbulence on smooth and rough walls. *Phys. Fluids* **15**, 35–46.

Raupach, M. R., Antonia, R. A. & Rajagopalan, S. 1991 Rough-wall turbulent boundary layers. *Appl. Mech. Rev.* **44**, 1–25.

Saddoughi, A. G. & Veeravalli, S. V. 1994 Local isotropy in turbulent boundary layers at high Reynolds numbers. *J. Fluid Mech.* **268**, 333–372.

Sabot, J., Saleh, I. & Comte-Bellot, G. 1977 Effects of roughness on the intermittent maintenance of Reynolds shear stress in pipe flow. *Phys. Fluids* **20**, 10, S150–S155

Shafi, H. S. & Antonia, R. A. 1995 Anisotropy of the Reynolds stresses in a turbulent boundary layer on a rough wall. *Exps. Fluids* **18**, 213–215.

Smalley, R. J., Antonia, R. A. & Djenidi, L. 2001 Self-preservation of rough-wall turbulent boundary layers. *Eur. J. Mech.* B **20**, 591–602.

Smalley, R. J., Leonardi, S., Antonia, R. A., Djenidi, L. & Orlandi, P. 2002 Reynolds stress anisotropy of turbulent rough wall layers. *Exps. Fluids* **33**, 31–37.

Smith, R. W. 1994 Effect of Reynolds number on the structure of turbulent boundary layers. PhD thesis, Princeton University.

Song, S. & Eaton, J. K. 2002 The effects of wall roughness on the separated flow over a smoothly contoured ramp. *Exps. Fluids* **33**, 38–46.

Spalart, P. R. 1988 Direct simulation of a turbulent boundary layer up to $R_\theta = 1410$. *J. Fluid Mech.* **187**, 61–98.

Tachie, M. F., Bergstrom, D. J. & Balachandar, R. 2000 Rough wall turbulent boundary layers in shallow open channel flow. *Trans. ASME*: *J. Fluids Engng* **122**, 533–541.

Tani, I. 1987 Turbulent boundary layer development over rough surfaces. In *Perspectives in Turbulence Studies* (ed. H. U. Meier & P. Bradshaw), pp. 223–249. Springer.

Tamura, T., Cao, S., Tsobokura, M., Tateyama, Y. & Inaba, T. 2003 LES analysis on dispersion in surface layer over randomly arranged roughness blocks. In *Proc. 3rd Intl Symp. on Turbulence and Shear Flow Phenomena, Sendai, Japan* (ed. N. Kasagi, J. K. Eaton, R. Friedrich, J. A. C. Humphrey, M. A. Leschziner & T. Miyauchi), pp. 353–358.

Townsend, A. A. 1961 Equilibrium layers and wall turbulence. *J. Fluid Mech.* **11**, 97–120.

Townsend, A. A. 1976 *The Structure of Turbulent Shear Flow. 2nd Edn.* Cambridge University Press.

Tremblay, F., Manhart, M. & Friedrich, R. 2001 DNS and LES of flow around a circular cylinder at subcritical Reynolds number with Cartesian grids. In *LES of Complex Transitional and Turbulent Flows* (ed. R. Friedrich & W. Rodi), pp. 133–150. Kluwer.